DOI: 10.31265/atnrs.773

High Definition 2-dimensional Numerical Model of Particle Settling on Newtonian and Shear-Thinning Fluids

Lucas P. Volpi[1,2], Eric Cayeux[2], Rune W. Time[1]

[1]University of Stavanger, Kjell Arholms gate 41, 4021 Stavanger, Norway
[2]NORCE, Professor Olav Hanssens vei 15, 4021 Stavanger, Norway

ABSTRACT

Well-defined particle sedimentation can provide relevant information in characterizing non-colloidal suspension. Nonetheless, the interaction between phases can become extremely convoluted as agglomerates are formed and broken, dynamically creating regions of high and low shear-rate. Numerical simulations are an alternative to obtain detailed descriptions of said interactions. In this work, the lattice-Boltzmann method is used together with the discrete element method to solve for two-dimensional sedimentation problems for both Newtonian and shear-thinning fluids.

INTRODUCTION

The presence of particles in a fluid can directly affect the observed rheological behaviour. Particle agglomerates can change local observation, while the flow itself can affect the agglomerate's structure. In general, the settling velocity is a key parameter in characterizing the non-colloidal solution.[1]

In the case of the settling, where the system is driven by the disturbances on the fluid due to the dynamic of the particles, this interaction becomes complex, as the coupling becomes more evident. Other parameters, as the degree of polydispersity can directly affect the settling process as well as the formation and maintainment of aggregates.[2] Simultaneously, the formation of agglomerates also depend on the rheological behviour. Shear-thinning viscosity, viscoelasticity and thixotropy directly affects the formation of the agglomerates.[3]

To do so, Eulerian-Lagrangian methods are well suited, as they can provide information on the particle's behaviour individually. Nonetheless, traditional finite volume and finite difference methods require a numerical discretization rougher than the actual particle size[4] and the interaction with the fluid is commonly associated with empirical models, such as drag forces.[5] The lattice-Boltmzann method (LBM) then becomes an alternative, as it inherently needs lattice sizes smaller then the solid boundaries, which leads to higher discretization, at the cost of higher computational cost. Chen et al., for example, used the LBM together with discrete elements to model two-dimensional suspension in Newtonian fluids.[6]

In this work, the four-way coupled lattice-Boltzmann-discrete-element method is used to model a two-dimensional monodispersed suspension settling case through direct numerical simulation (DNS) for both Newtonian and shear-thinning fluids. This allows to obtain highly descriptive solutions of the flow in-between the agglomerates.

MODELS & METHODS

In order to model the particle settling, a combination of the lattice-Boltzmann and discrete element (DEM) methods is used. The former consists on a mesoscopic approach to solve the Navier-Stokes equations. When Multiple Relaxation Time operator is used,[7,8] the method is expressed as:

$$f_i(\vec{\mathrm{x}} + \vec{\mathrm{c}}_i\Delta t, t + \Delta t) - f_i(\vec{\mathrm{x}}, t) = \sum_j \omega_{ij}(f_j^{(\mathrm{eq})} - f_j). \tag{1}$$

where f_i is the density distribution function, $f_i^{(\mathrm{eq})}$ is the equilibrium function, ω_{ij} are the terms of the matrix $\underline{\underline{\omega}}$ which contains the collision operators. The indices i and j depend on the velocity sets used (lv). In this case, 9 velocity sets are used for the two-dimensional model, known as D2Q9.

The collision operator matrix is better described in the momentum base as $\underline{\underline{\omega}} = \underline{\underline{\mathrm{M}}}^{-1}\underline{\underline{\Lambda}}\ \underline{\underline{\mathrm{M}}}$ where $\underline{\underline{\mathrm{M}}}$ is an orthonormal base for the momentum transformation[7] as to obtain a diagonal matrix for $\underline{\underline{\Lambda}}$. In practice, the equilibrium function is calculated directly in the momentum base as: $\vec{\mathrm{m}} = \underline{\underline{\mathrm{M}}}\ \vec{\mathrm{f}}^{(\mathrm{eq})}$. The main diagonal of $\underline{\underline{\Lambda}}$ is composed by $\mathrm{diag}(\underline{\underline{\Lambda}}) = \{0\ \lambda_e\ \lambda_\epsilon\ 0\ \lambda_q\ 0\ \lambda_q\ \lambda_\nu\ \lambda_\nu\}$, each different λ is related to a respective moment. In particular, λ_e is related to the bulk viscosity and λ_ν with the kinematic viscosity. As the flow is considered incompressible, bulk viscosity effects are disregarded and λ_e, λ_q and λ_ϵ are chosen to provide stability, through empirical testing.[9] The last term is dependent on the viscosity, the time-step (Δt), and on the lattice sound-speed (c_s): $\nu = c_s^2\left(\frac{1}{\Delta t\,\lambda_\nu} - \frac{1}{2}\right)$.

To account for the solid phase, the partially saturated method (PSM) is used,[10] which modifies the collision operator for a smooth transition to the solid region: $f_i(\vec{\mathrm{x}} + \vec{\mathrm{c}}_i\Delta t, t + \Delta t) - f_i(\vec{\mathrm{x}}, t) = (1-\beta)\sum_j[\omega_{ij}(f_j^{(\mathrm{eq})} - f_j)] + \beta\ \mathcal{C}_\mathcal{S}$, where β is a transition coefficient dependent on the volume fraction, α. Here, it is chosen as:[10]

$$\beta(\vec{\mathrm{x}}, t) = \frac{\alpha(\vec{\mathrm{x}}, t)\ [\lambda_\nu^{-1} - 0.5]}{1 - \alpha(\vec{\mathrm{x}}, t) + [\lambda_\nu^{-1} - 0.5]}. \tag{2}$$

The solid collision operator is hereby chosen as:[10]

$$\mathcal{C}_\mathcal{S} = f_i^{(\mathrm{eq})}(\rho, \tilde{\vec{\mathrm{v}}}_\mathcal{S}) - f_i(\vec{\mathrm{x}}, t) + (1 - \lambda_\nu)[f_i(\vec{\mathrm{x}}, t) - f_i^{(\mathrm{eq})}(\rho, \vec{\mathrm{v}})]. \tag{3}$$

Whereas there are several collision operators, this provides good stability[11] for $\lambda_\nu \to \frac{1}{2}$, at the cost of sub-optimal convergence when compared with other methods.[12] The solid velocity field is calculated through averaging all the particles within the same lattice,[13] $\tilde{\vec{\mathrm{v}}}_\mathcal{S} = \frac{\sum_{n=0}^{N}\alpha^{(\mathrm{n})}\vec{\mathrm{v}}_\mathcal{S}^{(\mathrm{n})}}{\sum_{n=0}^{N}\alpha^{(\mathrm{n})}}$, where the superscript (n) indicates the n^{th} particle that share a same lattice in $\vec{\mathrm{x}}$ and $\vec{\mathrm{v}}_\mathcal{S}$ is the field description of the solid velocity.

The fluid forces and torques at the n^{th} particle can be calculated as:[10]

$$\vec{\mathrm{F}}_f^{(\mathrm{n})} = \frac{\Delta x^2}{\Delta t}\sum_\mathcal{S}\left[\beta(\vec{\mathrm{x}}_\mathcal{S})\sum_i \vec{\mathrm{c}}_i\,\mathcal{C}_{i,\mathcal{S}}\right]; \quad \vec{\mathrm{T}}_f^{(\mathrm{n})} = \frac{\Delta x^2}{\Delta t}\sum_\mathcal{S}\left\{[(\vec{\mathrm{x}}_\mathcal{S} - \vec{\mathrm{p}}_n)\beta(\vec{\mathrm{x}}_\mathcal{S})]\sum_i \vec{\mathrm{c}}_i\,\mathcal{C}_{i,\mathcal{S}}\right\}, \tag{4}$$

where $\vec{x}_S$ is the solid-covered region and $\vec{p}_n$ is the particle's geometrical centre position. As the model is two-dimensional, the hydraulic force is a distribution along the disregarded direction. This way, the force is corrected by assuming that it affects a cylindrical shape of height $h = 2R$, and that the projected area is truly spherical. Thus, the force is corrected by: $2RA_{cyl}/A_{sphere} = 2R/\pi$.

The particles themselves are modelled through:

$$m_n\ddot{\vec{p}}_n = \sum_m \vec{F}_{mn} + \vec{F}_w + \vec{F}_f - \Delta m\vec{g}; \quad I_n\dot{\vec{\omega}}_n = \sum_m \vec{T}_{mn} + \vec{T}_w + \vec{T}_f, \tag{5}$$

where m_n and I_n are intertial terms, $\vec{F}_{mn}$ and $\vec{T}_{mn}$ come from the interaction with other particles, $\vec{F}_w$ and $\vec{T}_w$ are due to collision with the wall, and $\Delta m\vec{g}$ is the effective weight considering buoyancy effects. Finally, $\dot{\vec{\omega}}$ is the rotational speed. The interaction forces are considered to be of a linear spring-damper type[14] during contact.

Two different rheological behaviours are considered: (i) a Newtonian fluid and a (ii) shear-thinning fluid which follows a Quemada[15] model: $\nu = \nu_\infty\left[\frac{1+\Gamma^p}{\chi+\Gamma^p}\right]^2$, with $\Gamma = \frac{\dot{\gamma}}{\dot{\gamma}_c}$.

RESULTS

In this section, the simulation procedure is shown as well as the results obtained. The relaxation parameters are set to $\lambda = 1$, with exception of λ_ν, which depends on the viscosity. For the non-Newtonian case, the relaxation parameter is adjusted every time-step.[16] For the Newtonian case, several simulations with a single particle were conducted until a lattice velocity $\Delta x/\Delta t$ yielded a relaxation parameter λ_ν where the terminal velocity matched the expected value. This lattice velocity was then used for the shear-thinning case as well.

The characteristic times for the LBM and DEM can differ, thus, a sub-loop scheme is adopted, where several DEM integrations are conducted through one LBM step. In this case, a predictor-corrector scheme is used for the DEM.[4] The lattice size Δx was set to be smaller then the particle, with $R/\Delta x > 5$, where R is the particle radius.

The stiffness coefficients are considered to be large enough to avoid large overlaps but small enough to allow large time-steps.[4]

The fluid domain consists in a rectangular area with width $w = 80$mm and height $w = 160$mm. All the particles are initially organized in a rectangle with half the total width. The particles are mono-dispersed with a radius of $R = 0.5$ mm. The particle density was set to match glass beads, and is $\rho_s = 2650$ [kg/m^3]. The Newtonian fluid is a 9:1 glycerin-water mixture, which resulted in a viscosity of 0.209 [Pa·s] and a density of $\rho_{f,Newt} = 1234$ [kg/m^3]. The shear-thinning fluid, on the other hand, had $\rho_{f,st} = 1101$ [kg/m^3], $\nu_\infty = 0.0236$ [Pa·s], $\dot{\gamma}_c = 273.94$ [1/s], $p = 0.436$ and $\chi = 10^{-6}$.

In Fig. 1, the simulation for the Newtonian fluid is shown. In this case, the particles are divided into two groups, left-side, and right-side. The former is shown in a red color gradient whereas the latter is a cyan color gradient. The innermost section is of a darker shade, whereas the outer most lighter. The color and arrow fields characterize the velocity – magnitude and direction. The insert region at the top shows the y-velocity of each particle along its position in relation to the x-axis for the whole particle domain.

Similarly, the simulation of the shear-thinning suspension is shown in Fig. 2, where different stages of development are shown. The shear-rate field is presented in Fig. 3. The figure is zoomed in around the particle cluster.

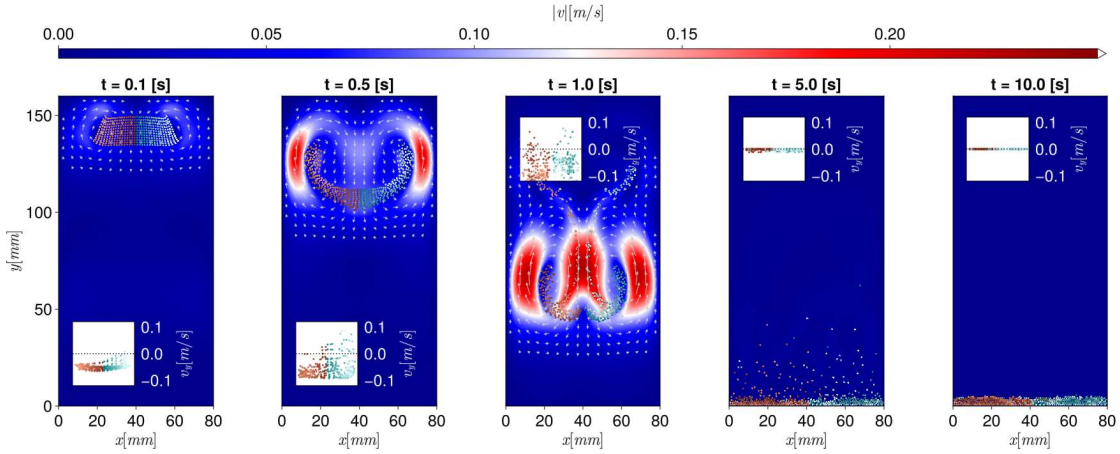

FIGURE 1: Vertical velocity field for $t = 0.1$s, 1s, 5s and 10s for a Newtonian fluid. The particles on the left follow a cyan color-gradient and on the right a red color-gradient. insert plots refer to the vertical velocity distribution of the particles.

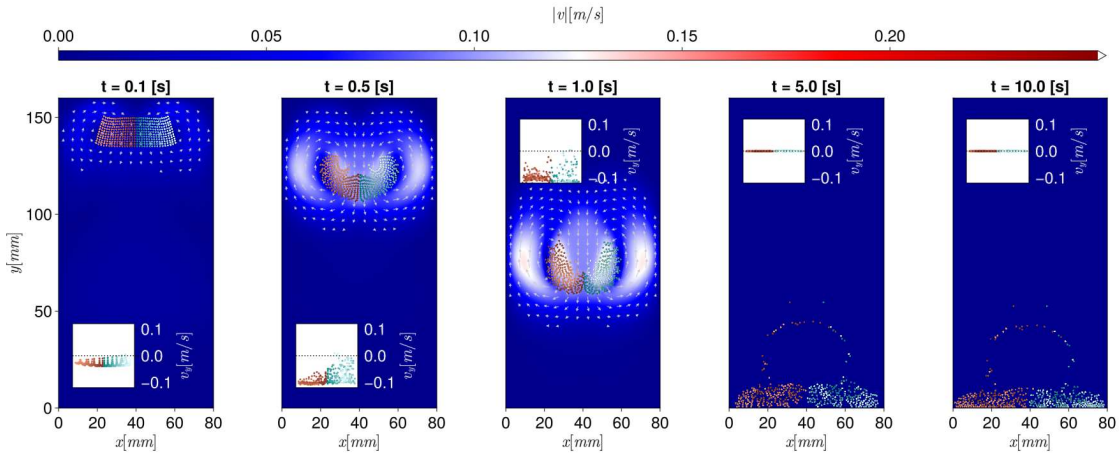

FIGURE 2: Vertical velocity field for $t = 0.1$s, 1s, 5s and 10s for a shear-thinning fluid. The particles on the left follow a cyan color-gradient and on the right a red color-gradient. insert plots refer to the vertical velocity distribution of the particles.

DISCUSSION

In this section, the results shown previously are discussed. From the Newtonian case, shown in Fig. 1, it can be seen that the particles on the right and the left almost do not mix. However, each of the halves shows inner rotation within the agglomerate structure. The centre of the agglomerate has a larger pressure, which causes it to split. The velocity profile of the particles is not perfectly symmetric, possibly of numerical nature, such as asymmetries due to mesh-particle overlap, which can affect the area fraction.

As the shear-thinning fluid is simulated, a similar behaviour is observed. However, the agglomerate does not detach vertically. The same splitting in the centre is seen as well as strong inner rotation in the particle phase. As a particle separate from the main group, it, by itself, does not carry enough weight and size to affect the shear-rate field, thus, the large viscosities are able to break the fall, even though not at a full stop. In the last

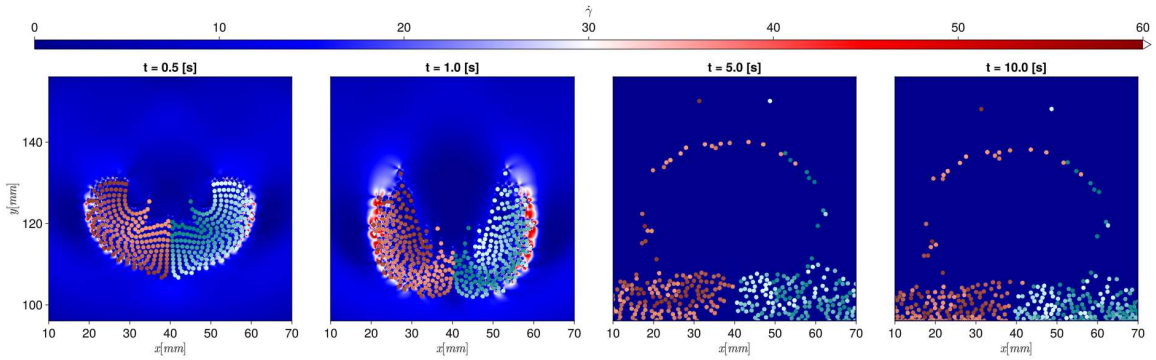

FIGURE 3: Shear-rate field for $t = 0.5$s, 1s, 5s and 10s for a shear-thinning fluid. The particles on the left follow a cyan color-gradient and on the right a red color-gradient.

five seconds, a ring-like configuration is produced by said particles. At the same time, the proximity to the wall also increases the shear-thinning viscous effects, which delays significantly the sedimentation of the particles.

CONCLUDING REMARKS

In this work, the particle settling problem is explored. The lattice-Boltzmann method is coupled with the discrete element method and a two-dimensional model is provided. The expected physical behaviour is observed, with the particle dynamics as well as the flow fields inside the particle agglomerates. On the presence of a shear-thinning fluid, as soon as the particles separate from the main cloud body, they apparently get stuck in the high-viscosity zone as their own weight is not enough to cause large perturbations of the field, which causes them to slow down. In the future, three-dimensional behaviour can be evaluated as well as viscoelastic models.

REFERENCES

1. Hajir Kourki and Mohammad Hossein Navid Famili. Particle sedimentation: Effect of polymer concentration on particle-particle interaction. *Powder Technology*, 221:137–143, 2012.

2. Gustavo Coelho Abade and Francisco Ricardo Cunha. Computer simulation of particle aggregates during sedimentation. *Computer Methods in Applied Mechanics and Engineering*, 196(45-48):4597–4612, 2007.

3. Zhaosheng Yu, Anthony Wachs, and Yannick Peysson. Numerical simulation of particle sedimentation in shear-thinning fluids with a fictitious domain method. *Journal of Non-Newtonian Fluid Mechanics*, 136(2-3):126–139, 2006.

4. Hamid Reza Norouzi, Reza Zarghami, Rahmat Sotudeh-Gharebagh, and Navid Mostoufi. *Coupled CFD-DEM modeling: formulation, implementation and application to multiphase flows*. John Wiley & Sons, 2016.

5. Bruno Blais, Manon Lassaigne, Christoph Goniva, Louis Fradette, and François Bertrand. Development of an unresolved CFD-DEM model for the flow of viscous sus-

pensions and its application to solid-liquid mixing. *Journal of Computational Physics*, 318:201–221, 2016.

6. Hongsheng Chen, Wenwei Liu, Zhiwei Chen, and Zhong Zheng. A numerical study on the sedimentation of adhesive particles in viscous fluids using LBM-LES-DEM. *Powder Technology*, 391:467–478, 2021.

7. Dominique d'Humieres. Generalized lattice-boltzmann equations. *Rarefied gas dynamics*, 1992.

8. Dominique D'Humières, Irina Ginzburg, Manfred Krafczyk, Pierre Lallemand, and Li Shi Luo. Multiple-relaxation-time lattice Boltzmann models in three dimensions. In *Philosophical Transactions of the Royal Society A: Mathematical, Physical and Engineering Sciences*, volume 360, pages 437–451, mar 2002.

9. Krüger Timm, Halim Kusumaatmaja, Alexandr Kuzmin, O Shardt, G Silva, and E Viggen. The lattice boltzmann method: principles and practice. *Cham, Switzerland: Springer International Publishing AG*, 2016.

10. D. R. Noble and J. R. Torczynski. A lattice-boltzmann method for partially saturated computational cells. *International Journal of Modern Physics C*, 9(8):1189–1201, 1998.

11. Tim Najuch and Jin Sun. Analysis of two partially-saturated-cell methods for lattice Boltzmann simulation of granular suspension rheology. *Computers and Fluids*, 189:1–12, 2019.

12. C. Rettinger and U. Rüde. A comparative study of fluid-particle coupling methods for fully resolved lattice Boltzmann simulations. *Computers and Fluids*, 154:74–89, 2017.

13. Pei Zhang, S. A. Galindo-Torres, Hongwu Tang, Guangqiu Jin, A. Scheuermann, and Ling Li. An efficient Discrete Element Lattice Boltzmann model for simulation of particle-fluid, particle-particle interactions. *Computers and Fluids*, 147:63–71, 2017.

14. Peter A Cundall and Otto DL Strack. A discrete numerical model for granular assemblies. *Geotechnique*, 29(1):47–65, 1979.

15. D Quemada. Rheological modelling of complex fluids. i. the concept of effective volume fraction revisited. *The European Physical Journal-Applied Physics*, 1(1):119–127, 1998.

16. Zhenhua Chai, Baochang Shi, Zhaoli Guo, and Fumei Rong. Multiple-relaxation-time lattice Boltzmann model for generalized Newtonian fluid flows. *Journal of Non-Newtonian Fluid Mechanics*, 166(5-6):332–342, 2011.

17. Simon Danisch and Julius Krumbiegel. Makie.jl: Flexible high-performance data visualization for Julia. *Journal of Open Source Software*, 6(65):3349, 2021.

Acknowledgments

This research was funded by the Norwegian Research Council, Equinor and Sekal. Figures were generated with the Makie package.[17]